Communications in Nonlinear Science and Numerical Simulation 118 (2023) 107015

Contents lists available at ScienceDirect

Communications in Nonlinear Science and Numerical Simulation

journal homepage: www.elsevier.com/locate/cnsns

Research paper

A novel 1D-FDTD scheme to solve the nonlinear second-order thermoviscous hydrodynamic model

Isidro Villó-Pérez [a], Pedro-María Alcover-Garau [b,*], María Campo-Valera [b], Rafael Toledo-Moreo [a]

[a] Department Electronics and Computer Technology and Projects, Universidad Politécnica de Cartagena, Spain
[b] Department of Information and Communication Technologies, Universidad Politécnica de Cartagena, Spain

ARTICLE INFO

Article history:
Received 11 July 2022
Received in revised form 10 October 2022
Accepted 12 November 2022
Available online 17 November 2022

Keywords:
Nonlinear acoustic in thermoviscous fluid
FDTD methods
Abstract data types
Numerical simulation

ABSTRACT

In this paper, we present a novel and simple Yee Finite-Difference Time-Domain (FDTD) scheme to solve numerically the nonlinear second-order thermoviscous Navier–Stokes and the Continuity equations. In their original form, these equations cannot be discretized by using the Yee's mesh, at least, easily. As it is known, the use of the Yee's mesh is recommended because it is optimized in order to obtain higher computational performance and remains at the core of many current acoustic FDTD softwares. In order to use the Yee's mesh, we propose to rewrite the aforementioned equations in a novel form. To achieve this, we will use the substitution corollary. This procedure is novel in the literature. Although the scheme can be extended to more than one dimension, in this paper, we will focus only on the one-dimensional solution because it can be validated with two analytical solutions to the Burgers equation: the Mendousse mono-frequency solution and the Lardner bi-frequency solution. Numerical solutions are excellently consistent with the analytical solution, which demonstrates the effectiveness of our formulation.

1. Introduction

The acoustic Yee Finite Difference Time Domain (FDTD) method has become one of the most effective tools for the numerical solution of linear and nonlinear acoustic problems because of its mathematical appeal, conceptual simplicity, easy implementation, and relative low computational costs. The method was first developed in the electromagnetic area by Kane Shee-Gong Yee in 1966 in order to study the scattering of electromagnetic waves [1]. In 1994, Botteldooren adapted this method to solve linear acoustic problems in lossless media using a quasi-Cartesian grid [2]. In 1996, the same author extended the algorithm to include second-order nonlinear effects, heat conduction, and damping [3]. Since then, the rapid growth of the literature on the subject has been an indication of its general acceptance. In fact, the method has been used in applications such as: room acoustics [4,5], environmental acoustics [6], sound diffusers [7], and ultrasounds [8–11], among others.

The purpose of this paper is to present a novel and simple Yee FDTD scheme to solve numerically the nonlinear second-order thermoviscous Navier–Stokes and the Continuity equations for the unknowns $\vec{u}$ (particle velocity) and p (pressure). In their original form, these equations cannot be discretized by using the Yee's mesh. As is known, the Yee's mesh is

* Correspondence to: Universidad Politécnica de Cartagena, Campus Muralla del Mar, s/n, Cartagena, E-30202, Spain.
E-mail addresses: isidro.villo@upct.es (I. Villó-Pérez), pedro.alcover@upct.es (P.-M. Alcover-Garau), maria.campo@upct.es (M. Campo-Valera), rafael.toledo@upct.es (R. Toledo-Moreo).

https://doi.org/10.1016/j.cnsns.2022.107015

optimized in order to obtain higher computational performance. It has been proved that it is a very robust technique and remains at the core of many current FDTD softwares. So, the use of the Yee's mesh is recommended.

In order to use Yee's mesh, we propose to rewritten the nonlinear second-order thermoviscous Navier–Stokes and Continuity equations in a more convenient form. To achieve this, we will use the *substitution corollary* which tells us: any second-order relation may be substituted by its first order approximation, since the resulting error is of third order. This procedure is novel in the literature and has the following advantages:

(i) The novel equations are found to be easy to implement by using FDTD method based on the Yee's mesh.
(ii) The viscosity and thermal conductivity can be dealt with directly.
(iii) The resulting algorithm is fast and accurate, and it allows us to obtain simultaneously the particle velocity $\vec{u}$ and pressure p at low computational cost.

Although the scheme can be extended to more than one dimension, in this paper we will focus on the one-dimensional solution. This will allow to compare the numerical solution with analytical solutions, as well as to do a brief and understandable review of the more significant effects in nonlinear acoustics, such us: *harmonic generation* and *difference-frequency generation*. Furthermore, we have implemented the algorithm in our own C++ code optimized for very short execution times.

This work is organized as follows: Section 2 presents the conventional formulation of the second-order hydrodynamic equations including viscosity and thermal conductivity. With this system of equations, the Westervelt and Burgers equations are obtained. Then, by using the *substitution corollary* the hydrodynamic equations are rewritten more conveniently. Section 3 deals with the methodology: derivation of numerical scheme. Section 4 considers the validation of our FDTD scheme using the Mendousse mono-frequency analytical solution and the Lardner bi-frequency analytical solution. This section also includes an estimative global error between both solutions using standard deviation as a metric. In Section 5, the authors includes the conclusions. Finally, we add an Appendix whose purpose is to schematize the mathematical formulation and the main points developed in the paper through the use of a conceptual map.

2. Problem formulation

2.1. Second-order hydrodynamic equations I

Let us start this section by writing the nonlinear second-order approximation thermoviscous hydrodynamic equations:

$$\rho_o \frac{\partial \vec{u}}{\partial t} + \vec{\nabla} p = -\frac{\mu_1}{\rho_o c_o^2} \frac{\partial}{\partial t} \left(\vec{\nabla} p \right) \tag{1}$$

$$\frac{\partial \rho}{\partial t} + \rho_o \vec{\nabla} \cdot \vec{u} = \frac{1}{\rho_o c_o^4} \frac{\partial p^2}{\partial t} \tag{2}$$

For a detailed derivation of this system of equations, the reader is referred to the book by Hamilton and Blackstock [12, equations (36) and (37) p.52] or Ref. [13]. Here, $\vec{\nabla}$ denotes the vector nabla operator, $\vec{u}(\vec{r}, t)$ is the acoustic particle velocity vector (which is assumed to be irrotational: $\vec{\nabla} \times \vec{u} = 0$), $p(\vec{r}, t)$ is the acoustic pressure and $\rho(\vec{r}, t)$ the acoustic mass density. As usual, an "o" subscript attached to a physical quantity denotes the equilibrium state value (which is assumed to be constant), more concretely: c_o is the small-signal sound speed (evaluated at the equilibrium state) and ρ_o the equilibrium mass density. Finally, to facilitate the notation, we have defined the viscosity term μ_1 or first loss term as:

$$\mu_1 = \mu_B + \frac{4}{3}\mu \tag{3}$$

where μ_B is the bulk viscosity and μ the shear viscosity.

Eqs. (1) and (2) are the second-order Navier–Stokes and Continuity equations, respectively. This system of equations has to be completed by the second-order equation of state (cf. Eq. (4)), which shows the relation between pressure and density (see [12, equation(40) p.53]):

$$\rho = \frac{p}{c_o^2} - \frac{1}{\rho_o c_o^4} \frac{B}{2A} p^2 - \frac{\mu_2}{\rho_o c_o^4} \frac{\partial p}{\partial t} \tag{4}$$

here $B/2A$ is the dimensionless parameter of nonlinearity and μ_2 is the second loss term which is due to the thermal conduction of the fluid and has been defined as:

$$\mu_2 = \kappa \left(\frac{1}{c_v} - \frac{1}{c_p} \right) \tag{5}$$

where κ is the thermal conductivity and c_v, c_p the specific heats at constant volume and constant pressure, respectively.

The system of Eqs. (1), (2), (4) govern the propagation of nonlinear acoustic waves in thermoviscous fluids. Now, if we substitute Eq. (4) into (2), the hydrodynamic equations can be written as a function of p and u only. On the other hand,

to simplify the notation, we define $\delta_1 = \mu_1/\rho_o$, $\delta_2 = \mu_2/\rho_o$. Therefore, Eqs. (1) and (2) can be rewritten and arranged in the form:

$$\frac{\partial \vec{u}}{\partial t} = -\frac{1}{\rho_o}\vec{\nabla} p - \frac{\delta_1}{\rho_o c_o^2}\frac{\partial}{\partial t}\left(\vec{\nabla} p\right) \tag{6}$$

$$\frac{\partial p}{\partial t} = -\rho_o c_o^2 \vec{\nabla}\cdot\vec{u} + \frac{\beta}{\rho_o c_o^2}\frac{\partial p^2}{\partial t} + \frac{\delta_2}{c_o^2}\frac{\partial^2 p}{\partial t^2} \tag{7}$$

where $\beta = 1 + B/2A$ is the coefficient of nonlinearity.

2.2. Westervelt and Burgers equations

As is well known, the Westervelt wave equation is one the fundamental equations in nonlinear acoustics [14]. This equation can be directly derived from the system of Eqs. (6), (7) solving for p. In fact, applying the divergence on (6), taking the partial derivative of (7) with respect to time and using the linear wave equation $\nabla^2 p = 1/c_o^2\ \partial^2 p/\partial t^2$, we can obtain the Westervelt equation (see [12, equation (46) p.55]):

$$\nabla^2 p - \frac{1}{c_o^2}\frac{\partial^2 p}{\partial t^2} = -\frac{\beta}{\rho_o c_o^4}\frac{\partial^2 p^2}{\partial t^2} - \frac{\delta}{c_o^4}\frac{\partial^3 p}{\partial t^3} \tag{8}$$

where the term $\delta = \delta_1 + \delta_2$ is the diffusivity of sound, which takes into account both loss terms: the viscosity and the thermal conduction of the fluid.

It is also known that, from the one-dimensional form of the Westervelt equation, the Burgers Eq. (9) is derived (see [12, equation (54) p.57]):

$$\frac{\partial p}{\partial z} = \frac{\beta p}{\rho_o c_o^3}\frac{\partial p}{\partial \tau} + \frac{\delta}{2c_o^3}\frac{\partial^2 p}{\partial \tau^2} \tag{9}$$

where $\tau = t - z/c_o$ is the retarded time. The Burgers equation is one of the most popular nonlinear one dimensional wave equations whose analytical and numerical solution is well known and documented in the literature. For a comprehensive historical overview, the reader is referred to [15] and [16] and the references contained there.

Normally, the dimensionless form of the Burgers equation (see, for example, [17, equation (2.76)]) is more used than the above equation. However, we will use the dimensional Eq. (9) as a test to prove our numerical algorithm.

2.3. Second-order hydrodynamic equations II

For the purpose of this paper, we propose to rewrite Eqs. (6), (7) in a more convenient form. To achieve this, we use the so-called *substitution corollary* which tells us: any second-order relation may be substituted by its first order approximation, since the resulting error is of third order [12]. Therefore, it is legitimate to use the following linear (first-order) relations:

$$\frac{\partial}{\partial t}\left(\vec{\nabla} p\right) = -\rho_o c_o^2 \nabla^2 \vec{u}, \qquad \frac{\partial^2 p}{\partial t^2} = c_o^2 \nabla^2 p \tag{10}$$

Substituting these relations into Eqs. (6) and (7), and using the fact that $\partial p^2/\partial t = 2p\partial p/\partial t$, we can write:

$$\frac{\partial \vec{u}}{\partial t} = -\frac{1}{\rho_o}\vec{\nabla} p + \delta_1 \nabla^2 \vec{u} \tag{11}$$

$$\frac{\partial p}{\partial t} = -\rho_o c_o^2 \vec{\nabla}\cdot\vec{u} + \frac{2\beta}{\rho_o c_o^2} p\frac{\partial p}{\partial t} + \delta_2 \nabla^2 p \tag{12}$$

As shown below, writing the hydrodynamic model equations in this form is more suitable because it allows for direct and easy numerical discretization.

2.4. Reduction of hydrodynamic equations to 1D

For a $\hat{z}$-directed, with no variations in the $\hat{x}$ and $\hat{y}$ directions, i.e. $\frac{\partial}{\partial x} = \frac{\partial}{\partial y} = 0$; the system of Eqs. (11), (12) reduces down to the one dimensional case:

$$\frac{\partial u_z}{\partial t} = -\frac{1}{\rho_o}\frac{\partial p}{\partial z} + \delta_1 \frac{\partial^2 u_z}{\partial z^2} \tag{13}$$

$$\frac{\partial p}{\partial t} = -\rho_o c_o^2 \frac{\partial u_z}{\partial z} + \frac{2\beta}{\rho_o c_o^2} p\frac{\partial p}{\partial t} + \delta_2 \frac{\partial^2 p}{\partial z^2} \tag{14}$$

The system of equations above (13), (14) is essentially equivalent to the one dimensional Westervelt equation or its simplified version, the Burgers equation. Although both of these wave Eqs. (8) and (9) have been and are numerically

resolved in a large number of problems [18–22], their solution is not complete because the separate wave equation loses the structure relationship between p and u, i.e. the relationship between the amplitudes and the phases of the fields. On the contrary, the numerical solution of the system (13), (14) allows us to get the evolution of both physical quantities u and p simultaneously.

3. Methodology: Derivation of numerical scheme

To solve the system of equations numerically (13), (14), we first set the numerical solution domain $\Omega = \{(z,t) : z \in [0, z_{max}], t \in [0, t_{max})\}$ which is discretized into a space–time mesh defined by a set of integer and semi-integer nodes. In the classic Yee acoustic FDTD method [3], the field $u(z,t)$ is defined on integer nodes of the space–time whereas the field $p(z,t)$ is defined on semi-integer nodes. Namely:

$$u(z,t) = u(k\Delta z, n\Delta t) \equiv u^n(k) \tag{15}$$

$$p(z,t) = p\left[(k+1/2)\Delta z, (n+1/2)\Delta t\right] \equiv p^{n+1/2}(k+1/2) \tag{16}$$

where k and n are integer ($k = 0, 1, 2, \ldots, k_{max}$; $n = 0, 1, 2, \ldots, n_{max}$), and $\Delta z = z_{max}/k_{max}$ and $\Delta t = t_{max}/n_{max}$ are the spatial and temporal mesh sizes, respectively.

Now, let us define the following discrete operators:

$$I_u \cdot F(m_u) = \frac{F(m_u + 1/2) + F(m_u - 1/2)}{2} \tag{17}$$

$$D_u \cdot F(m_u) = \frac{F(m_u + 1/2) - F(m_u - 1/2)}{\Delta u} \tag{18}$$

$$D_u^2 \cdot F(m_u) = 4\frac{F(m_u + 1/2) - 2F(m_u) + F(m_u - 1/2)}{\Delta u^2} \tag{19}$$

with m_u an integer. The operator I_u is called *Centered Average Operator* (in the variable u), which is a second-order approximation in $\Delta u/2$ of the analytical identity operator, i.e. $F(m_u) = I_u \cdot F(m_u) + \mathcal{O}\left[(\Delta u/2)^2\right]$ Δ u/2. The operator D_u is called *Centered Difference Operator*, which is a second-order approximation of the analytical first-order derivative, i.e. $F'(m_u) = D_u \cdot F(m_u) + \mathcal{O}\left[(\Delta u/2)^2\right]$ Δ u/2. The operator D_u^2 is called *Second-Order Centered Difference Operator*, which is a second-order approximation of the analytical second-order derivative, i.e. $F''(m_u) = D_u^2 \cdot F(m_u) + \mathcal{O}\left[(\Delta u/2)^2\right]$ Δ u/2.

3.1. Time advancement equations

Using the operational language described above, we propose the following scheme, which is a second order approximation in $\Delta u/2$, to discretize the Eqs. (13), (14):

Scheme for Eq. (13):

$$\begin{aligned} D_t \cdot u_z^{n+1/2}(k) = &-\frac{1}{\rho_o} D_z \cdot p^{n+1/2}(k) + \\ &+ \delta_1\, I_z \cdot I_t \cdot D_z^2 \cdot u_z^{n+1/2}(k) \end{aligned} \tag{20}$$

Scheme for Eq. (14):

$$\begin{aligned} D_t \cdot p^n(k+1/2) = &-\rho_o c_o^2\, D_z \cdot u_z^n(k+1/2) + \\ &+ \frac{2\beta}{\rho_o c_o^2}\, I_t \cdot p^n(k+1/2)\, D_t \cdot p^n(k+1/2) + \\ &+ \delta_2\, I_z \cdot I_t \cdot D_z^2 \cdot p^n(k+1/2) \end{aligned} \tag{21}$$

where the centered average operator in (20) and (21) acts only on the terms where it is necessary to match the fields with the nodes of the space–time mesh.

Explicitly, the time advancement equations for u and p take the form:

- Time advancement equation for u:

$$\begin{aligned} u_z^{n+1}(k) = u_z^n(k) - C_1\left[p^{n+1/2}(k+1/2) - p^{n+1/2}(k-1/2)\right] + \\ + C_3\left[u_z^n(k+1) - 2u_z^n(k) + u_z^n(k-1)\right] \end{aligned} \tag{22}$$

- Time advancement equation for p:

$$p^{n+1/2}(k+1/2) = \frac{1 - \sqrt{1 - 4C_5 g(k,n)}}{2C_5} \tag{23}$$

where

$$g(k,n) = p^{n-1/2}(k+1/2) - \\ - C_2\left[u_z^n(k+1) - u_z^n(k)\right] - C_5\left[p^{n-1/2}(k+1/2)\right]^2 + \\ + C_4\left[p^{n-1/2}(k-1/2) - 2p^{n-1/2}(k+1/2) + p^{n-1/2}(k+3/2)\right] \tag{24}$$

The scheme holds five constants, which have been defined as:

$$C_1 = \frac{\Delta t}{\rho_o \Delta z}, \quad C_2 = \rho_o c_o^2 \frac{\Delta t}{\Delta z}, \quad C_3 = \frac{\delta_1}{2\rho_o c_o^2 \Delta z}, \\ C_4 = \frac{\delta_2 \Delta t}{\Delta z^2}, \quad C_5 = \frac{\beta}{\rho_o c_o^2} \tag{25}$$

Note that, the nonlinearity of the analytical equations involve a square root in the scheme as can be seen from Eq. (23).

3.2. Absorbing boundary condition

As is known, to simulate an unbounded spatial domain using a finite computational memory, it is necessary to apply absorbing boundary conditions (ABC) at the mesh borders. The simplest ABC is Mur's boundary condition which is obtained by discretizing the one-wave equation at the mesh borders [23]. For one dimensional problems, the Mur's boundary condition is a perfect absorber. Our scheme requires to apply ABC over both, pressure and velocity. On the right-hand side defined by the node k_{max}, the ABC is applied as follow:

$$u_z^{n+1}(k_{max}) = u_z^n(k_{max}-1) + \\ + C_6\left[u_z^{n+1}(k_{max}-1) - u_z^n(k_{max})\right] \tag{26}$$

$$p^{n+1/2}(k_{max}+1/2) = p^{n-1/2}(k_{max}-1/2) + \\ + C_6\left[p^{n+1/2}(k_{max}-1/2) - p^{n-1/2}(k_{max}+1/2)\right] \tag{27}$$

with C_6 a constant defined as:

$$C_6 = \frac{c_o \Delta t - \Delta z}{c_o \Delta t + \Delta z} \tag{28}$$

The boundary condition on the left-hand side can be derived similarly.

4. Validation: simulations and results

To validate the proposed FDTD scheme, the numerical results are compared with two analytical solutions to the Burger equation: the Mendousse mono-frequency solution and the Landner bi-frequency solution.

4.1. Validation with Mendousse solution

Consider the following boundary value problem for the Burgers equation:

$$\begin{cases} \dfrac{\partial p}{\partial z} = \dfrac{\beta p}{\rho_o c_o^3}\dfrac{\partial p}{\partial \tau} + \dfrac{\delta}{2c_o^3}\dfrac{\partial^2 p}{\partial \tau^2} \\ p(0,t) = P_o \sin \omega_o t \end{cases} \tag{29}$$

where the boundary condition is a harmonic mono-frequency function of amplitude P_o and frequency ω_o.

Mendousse obtained an analytical solution for this problem [24], which is expressed as a ratio of Bessel function series (see [12, equation(264)p.134]):

$$p(z,t) = -P_o \frac{4\Gamma^{-1}\sum_{n=1}^{\infty} n(-1)^n I_n\left(\frac{1}{2}\Gamma\right) e^{-n^2\alpha_o z}\sin\left[n\omega_o\left(t-\frac{z}{c_o}\right)\right]}{I_o\left(\frac{1}{2}\Gamma\right) + 2\sum_{n=1}^{\infty}(-1)^n I_n\left(\frac{1}{2}\Gamma\right) e^{-n^2\alpha_o z}\cos\left[n\omega_o\left(t-\frac{z}{c_o}\right)\right]} \tag{30}$$

where I_n is the modified Bessel function of the first kind and order n, α_o is the small-signal attenuation coefficient and Γ is the Goldberg number, both defined as:

$$\alpha_o = \frac{\delta\omega_o^2}{2c_o^3}, \qquad \Gamma = \frac{1}{\alpha_o z_{sh}} \tag{31}$$

being z_{sh} the shock distance:

$$z_{sh} = \frac{\rho_o c_o^3}{\beta P_o \omega_o} \tag{32}$$

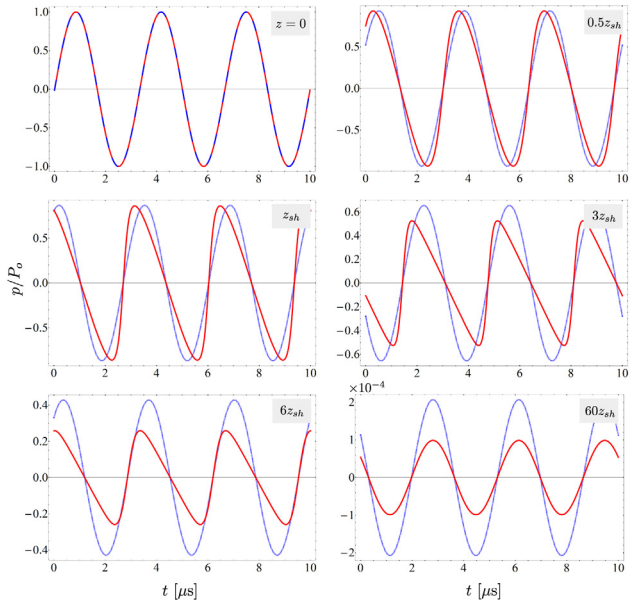

Fig. 1. Analytical time-dependent Mendousse solution (red curve) at various distances z for the following values: $c_o = 1500$ m/s, $\rho_o = 1000$ kg/m^3, $\beta = 10$, $\delta = 1.5 \cdot 10^{-3}$ m^2/s, $P_o = 1$ MPa and $f_o = 0.3$ MHz ($\omega_o = 2\pi f_o$). For these values $z_{sh} = 17.9049$ cm. The linear (first order) solution also is plotted in the figure (blue curve).

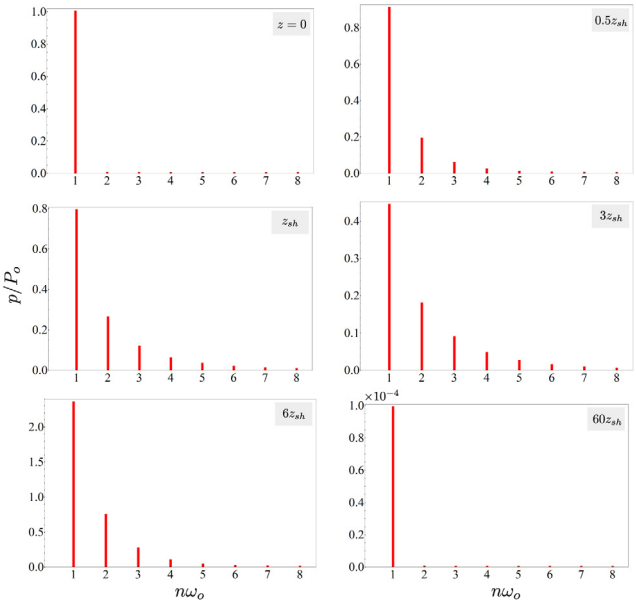

Fig. 2. Spectra components of the time series shown in Fig. 1.

Using the commercial software Wolfram Mathematica [25] we have plotted in Fig. 1 the time-dependent Mendousse solution (30) at various distances z using the values showed in the figure caption. We have chosen to set $\beta = 10$ in order to show the nonlinear effects in a short distance and, therefore to shorten the computational time in the numerical simulation. This figure shows the well known behavior of the progressive distortion of a nonlinear wave. During the propagation, the sinusoidal wave gradually develops a sawtooth profile (which is full at the distance $z = 3z_{sh}$). The sawtooth profile fades progressively until, after traveling a long distance, the wave returns to its original sinusoidal shape although much reduced in amplitude due to the effects of dissipation. This behavior is also observed in the frequency domain. Indeed, the progressive distorsion of the nonlinear wave involves the harmonics generation as shown in Fig. 2. Harmonics grow fast at first, later these decay until the fundamental mode ω_o with a strongly reduced amplitude.

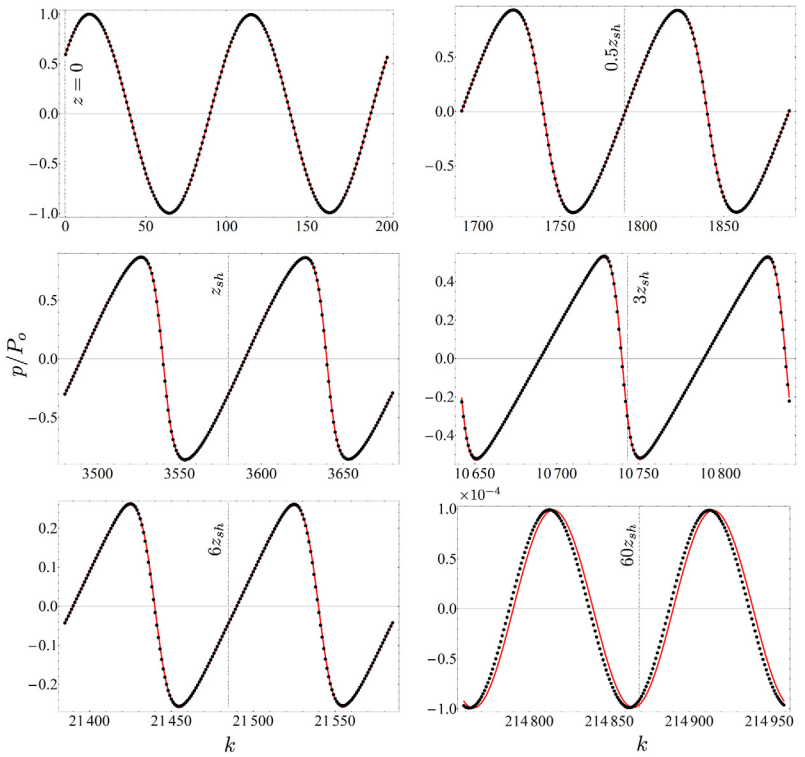

Fig. 3. Comparison between the numerical (black dots) and analytical (red curve) Mendousse solution along the direction of propagation $\hat{z}$. Parameters were set as in Fig. 1.

To compare the analytical solution shown in Fig. 1 (red curve) with the numerical solution obtained from the proposed scheme (22), (23), we take a numerical space domain of length $z_{max} = 61 z_{sh}$ ($z_{max} = 10.922$ m). The spatial mesh size is selected to be $\Delta z = \lambda / R_\lambda$ where R_λ is the number of samples per wavelength or numerical resolution in λ. The accuracy of the numerical solution depends on R_λ, and for an optimum result it is usually enough to take $R_\lambda = 20$ with λ the shorter wavelength implied in the problem. From Fig. 2, we can see that the harmonics generation involve the appearance of an infinite number of wavelengths but, above the fifth term, the contribution is negligible. So, we take $R_\lambda = 20$ and $\lambda = \lambda_o/5$ ($\lambda_o = c_o/f_o$) to set $\Delta z = 50$ μm. On the other hand, time step size is selected as $\Delta t = 0.9\Delta z/c_o = 30$ ns. With these values $k_{max} = z_{max}/\Delta z = 218440$. To ensure that the wave travels along the entire spatial domain from 0 to k_{max}, we have to take at least 242711 iterations. Fig. 3 shows the numerical solution (black dots) versus the analytical Mendousse solution (red curve) along the propagation direction $\hat{z}$ ($z = k\Delta z$). For the sake of simplicity, the space domain $[0, k_{max}]$ has been divided into six subintervals centered around the values $z = 0$, $0.5z_{sh}$, z_{sh}, $3z_{sh}$, $6z_{sh}$ and $60z_{sh}$ (corresponding to the observation planes in Fig. 1). It is important to note that at a very far distance from the origin (last panel in Fig. 3), the numerical solution suffers the well known phase-error or numerical dispersion. This error is inherent in any FDTD scheme and it is due to the difference between the numerical phase velocity and the real velocity [26].

In order to estimate a global error (absolute (*abs*) and relative (*rel*)) obtained to compare the numerical with the analytical solution, let us use the standard deviation σ as metric:

$$\sigma_{abs} = \sqrt{\frac{1}{N}\sum_{k=1}^{N}\left[(s_a(k) - s_n(k)) - \mu_{abs}\right]^2} \tag{33}$$

$$\sigma_{rel} = \sqrt{\frac{1}{N}\sum_{k=1}^{N}\left[\frac{s_a(k) - s_n(k)}{s_a(k)} - \mu_{rel}\right]^2} \tag{34}$$

where

$$\mu_{abs} = \frac{1}{N}\sum_{k=1}^{N}(s_a(k) - s_n(k)) \tag{35}$$

Table 1
Approximation errors in the Mendousse solution corresponding to panels in Fig. 3.

Panel: k in	μ_{abs}	σ_{abs}	μ_{rel}	σ_{rel}
[0, 200]	$-4.69615 \cdot 10^{-6}$	$8.85873 \cdot 10^{-4}$	$-2.4587 \cdot 10^{-3}$	$1.70759 \cdot 10^{-2}$
[1690, 1890]	$-2.04626 \cdot 10^{-6}$	$2.35083 \cdot 10^{-3}$	$-5.44085 \cdot 10^{-3}$	$5.23365 \cdot 10^{-2}$
[3480, 3680]	$-2.85154 \cdot 10^{-6}$	$6.04192 \cdot 10^{-3}$	$-1.13558 \cdot 10^{-2}$	$1.19867 \cdot 10^{-1}$
[10642, 10842]	$9.45146 \cdot 10^{-5}$	$7.06477 \cdot 10^{-3}$	$-1.82129 \cdot 10^{-2}$	$1.9583 \cdot 10^{-1}$
[21385, 21585]	$-1.18006 \cdot 10^{-6}$	$3.38684 \cdot 10^{-3}$	$-2.04512 \cdot 10^{-2}$	$2.2267 \cdot 10^{-1}$
[214759, 214959]	$-9.13433 \cdot 10^{-8}$	$1.07915 \cdot 10^{-5}$	$-2.90787 \cdot 10^{-1}$	2.37741

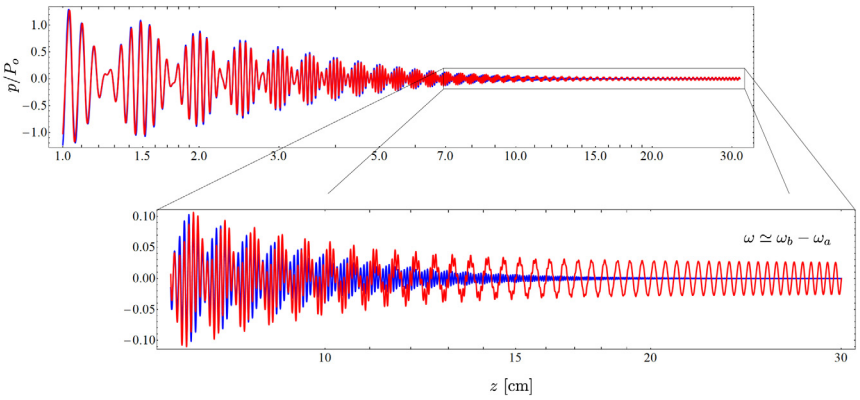

Fig. 4. Analytical Lardner solution (red curve) along the propagation direction $\hat{z}$ at $t = 0$. Parameters were set as following: $c_o = 1500$ m/s, $\rho_o = 1000$ kg/m^3, $\beta = 10$, $\delta = 1.5 \cdot 10^{-3}$ m^2/s, $P_o = 1$ MPa and $f_o = 0.1$ MHz ($\omega_o = 2\pi f_o$); $A = B = 1$, $a = 20$ ($\omega_a = a\omega_o$), $b = 23$, ($\omega_b = b\omega_o$). Blue curve is the lineal solution.

$$\mu_{rel} = \frac{1}{N}\sum_{k=1}^{N}\left(\frac{s_a(k) - s_n(k)}{s_a(k)}\right) \tag{36}$$

is the arithmetic mean (absolute (*abs*) and relative (*rel*)) with $s_a(k)$ and $s_n(k)$ the values for the analytical and numerical solutions at the node k, respectively.

Table 1 shows (μ, σ) for each panel in Fig. 3. Except for the phase error, we can conclude that the numerical solution is highly consistent with the analytical solutions, which demonstrates the effectiveness of the proposed numerical scheme.

All numerical computations were performed using C++ programming language and double-precision arithmetic on a CPU Intel i9-10900x (20) @4.500 Hz. Taking 218440 spatial nodes and 242711 iterations, the computational cost was of 5.66 min.

4.2. Validation with Lardner solution

We now consider the boundary value problem (29) but with the boundary bi-frequency condition:

$$p(0, t) = AP_o \sin(a\omega_o t) + BP_o \sin(b\omega_o t) \tag{37}$$

where A, B are real numbers, and a, b integer with $b > a$. The analytical solution for this problem was found by Lardner [27] in the form (a general multi-frequency solution can be found in [17,28]):

$$p(z, t) = -P_o \frac{2\Gamma^{-1}\sum_{l=-\infty}^{\infty}\sum_{m=-\infty}^{\infty} n_{lm}(-1)^{l+m}\mathcal{I}_{lm}e^{-n_{lm}^2\alpha_o z}\sin\left[(l\omega_a + m\omega_b)\left(t - \frac{z}{c_o}\right)\right]}{\sum_{l=-\infty}^{\infty}\sum_{m=-\infty}^{\infty}(-1)^{l+m}\mathcal{I}_{lm}e^{-n_{lm}^2\alpha_o z}\cos\left[(l\omega_a + m\omega_b)\left(t - \frac{z}{c_o}\right)\right]} \tag{38}$$

where $\omega_a = a\omega_o$, $\omega_b = b\omega_o$, $n_{lm} = al + bm$ and

$$\mathcal{I}_{lm} = I_l\left(\frac{A}{2a}\Gamma\right) I_m\left(\frac{B}{2b}\Gamma\right) \tag{39}$$

with Γ y α_o defined in (31). As in the Mendousse solution, I_n is the modified Bessel function of the first kind and order n.

For $A = B = 1$, $a = 20$ and $b = 23$, we have plotted in Fig. 4 the Lardner solution (38) at $t = 0$ and z in [0, 30] cm. For clarity in depiction, we have used logarithmic scale in the $\hat{z}$-axis in order to show the evolution of the wave along the propagation direction in the same diagram. The parameters used are shown in the figure caption.

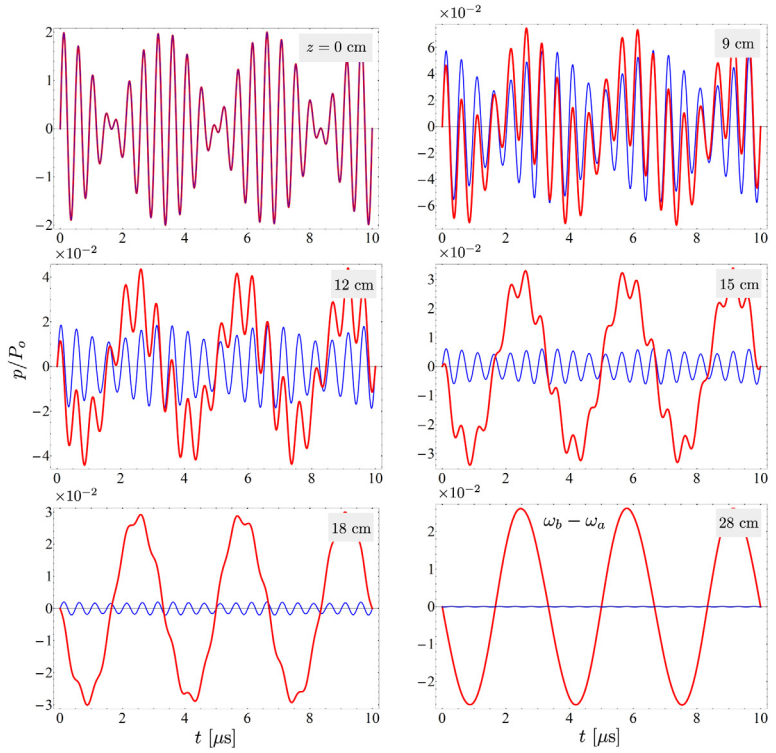

Fig. 5. Analytical time-dependent Lardner solution (red curve) at various distances z (see Fig. 4). As usual, blue curve is the lineal solution.

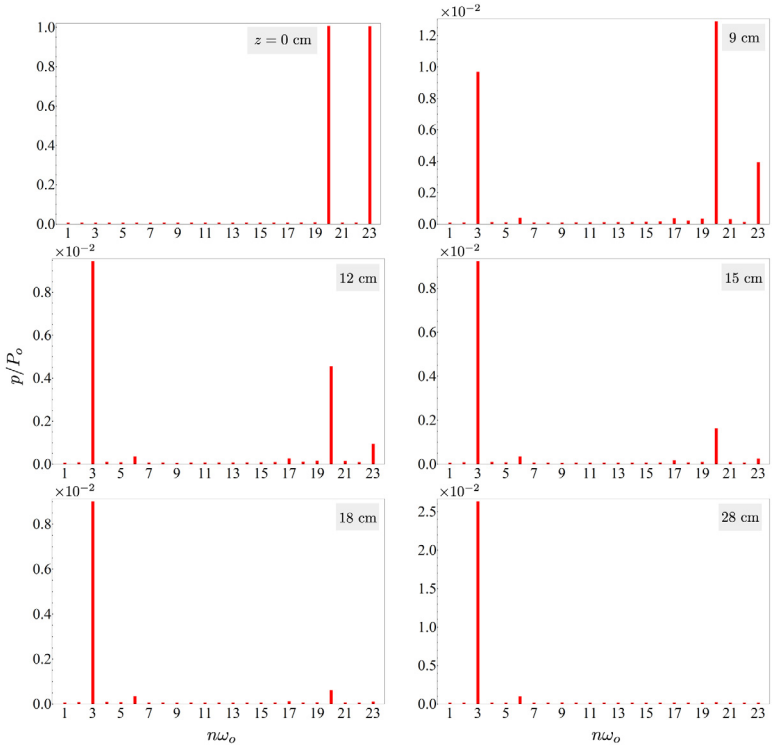

Fig. 6. Spectra components of the time series shown in Fig. 5.

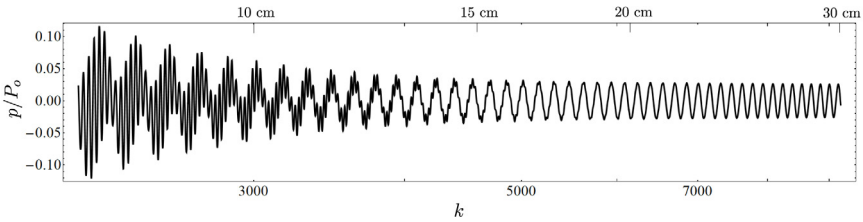

Fig. 7. Numerical Lardner solution along the propagation direction after 10222 iterations. Parameters were set as in Fig. 4.

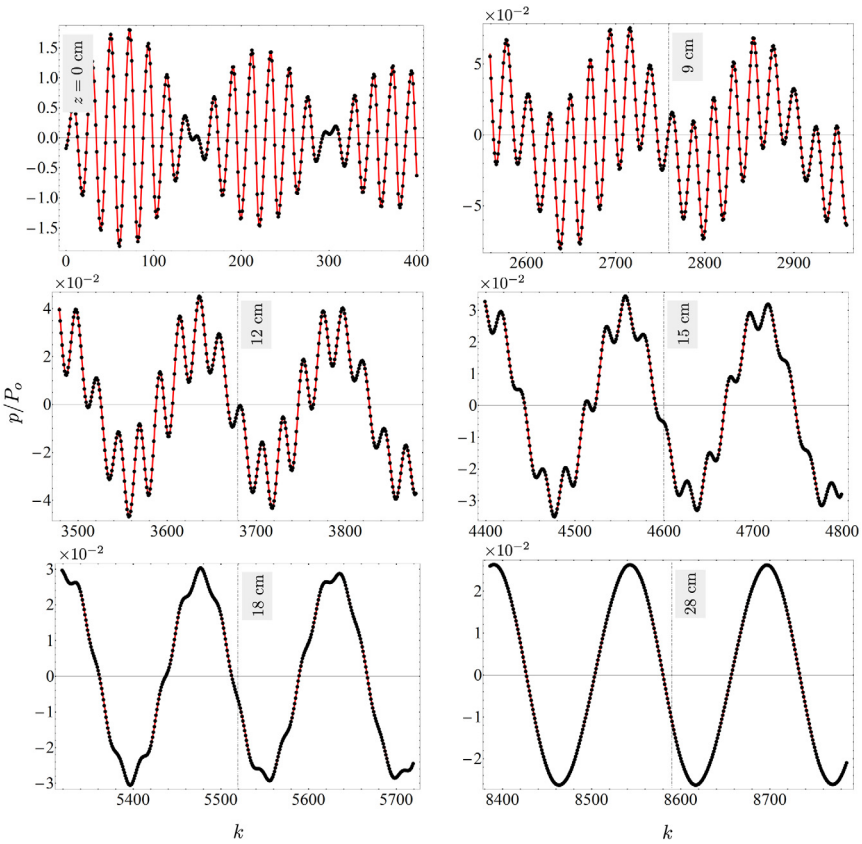

Fig. 8. Comparison between the numerical (black dots) and analytical (red curve) Lardner solution along the direction of propagation $\hat{z}$ ($z = k\Delta z$). Parameters were set as in Fig. 4.

Fig. 4 shows other classical phenomenon of nonlinear acoustics, known as difference-frequency generation: two nearby initial frequencies (ω_a, ω_b) create their difference-frequency $\omega_b - \omega_a$. In our example, near the distance $z = 28$ cm, the difference-frequency $(\omega_b - \omega_a = 3\omega_o)$ becomes dominant. The wave stays in this shape for a long distance until finally, all the energy not dissipated is transferred to the fundamental mode ω_o. This phenomenon is shown in major detail in Figs. 5 and 6. In Fig. 5 we have plotted the time-dependent Lardner solution at various distances z and in Fig. 6 their spectrums. These figures clearly show how the wave gradually develops the difference-frequency $3\omega_o$ along the propagation direction.

Let us now obtain the numerical Lardner solution using the FDTD scheme (22), (23). To do so, we take the space domain $z_{max} = 30$ cm. As is known, we have to sample to the shortest wavelength. Therefore, the spatial mesh size is set to be $\Delta z = \lambda_b / R_\lambda$ with $R_\lambda = 20$ and $\lambda_b = c_o/(\omega_b/2\pi)$ resulting $\Delta z = 32.6087$ μm. With these values, $k_{max} = z_{max}/\Delta z = 9199$. The time step size is selected to the value $\Delta t = 0.9\Delta z/c_o = 19.5652$ ns. After 10222 iterations, the wave has traveled the full space domain. Fig. 7 shows the numerical solution for k in [2146, 9199] (i.e. z in [7, 30] cm as in the zoom of Fig. 4).

The accuracy of the scheme is shown in Fig. 8 where we have plotted the numerical solution (black dots) versus analytical Lardner solution (red curve).

Error analysis shown in Table 2 indicates again that numerical results for Landner solution are consistent and accurate.

Table 2
Approximation errors in the Lardner solution corresponding to panels in Fig. 8.

Panel: k in	μ_{abs}	σ_{abs}	μ_{rel}	σ_{rel}
[0, 400]	$6.02984 \cdot 10^{-5}$	$8.48514 \cdot 10^{-3}$	$2.99538 \cdot 10^{-3}$	$7.56073 \cdot 10^{-2}$
[2559, 2959]	$4.1713 \cdot 10^{-5}$	$1.15461 \cdot 10^{-3}$	$-2.93475 \cdot 10^{-2}$	$3.11641 \cdot 10^{-1}$
[3479, 3879]	$2.61603 \cdot 10^{-5}$	$5.28597 \cdot 10^{-4}$	$9.60465 \cdot 10^{-3}$	$3.22338 \cdot 10^{-1}$
[4399, 4799]	$1.85882 \cdot 10^{-5}$	$2.46314 \cdot 10^{-4}$	$1.72706 \cdot 10^{-2}$	$4.93399 \cdot 10^{-1}$
[5319, 5719]	$1.50827 \cdot 10^{-5}$	$1.38296 \cdot 10^{-4}$	$9.6298 \cdot 10^{-3}$	$2.50851 \cdot 10^{-1}$
[8386, 8786]	$1.2029 \cdot 10^{-5}$	$9.59782 \cdot 10^{-5}$	$-5.20627 \cdot 10^{-3}$	$6.17032 \cdot 10^{-2}$

5. Conclusions

In this paper, we have proposed a novel FDTD scheme to solve the nonlinear second-order thermoviscous hydrodynamic model in one dimension. The numerical results obtained show good agreement with the analytical solutions. Therefore, the present scheme is an alternative way to solve the one dimensional Westervelt wave equation (or its simplified version: the Burgers equation) numerically. Our scheme can be considered to be competitive and worth recommending for its simplicity, accuracy and speed.

CRediT authorship contribution statement

Isidro Villó-Pérez: Conceptualization, Writing – original draft, Formal analysis, Writing – review & editing. **Pedro-María Alcover-Garau:** Software, Validation, Data curation, Writing – review & editing. **María Campo-Valera:** Investigation. **Rafael Toledo-Moreo:** Writing – review & editing.

Declaration of competing interest

The authors declare that they have no known competing financial interests or personal relationships that could have appeared to influence the work reported in this paper.

Data availability

Data will be made available on request.

Acknowledgments

This work was partially supported by the "Research Programme for Groups of Scientific Excellence at Region of Murcia" of the Seneca Foundation (Agency for Science and Technology of the Region of Murcia, Spain - 19895/GERM/15). María Campo-Valera is grateful for postdoctoral program Margarita Salas - Spanish Ministry of Universities (financed by European Union - NextGenerationEU).

Appendix

In this appendix we schematize the mathematical formulation and the main points developed in the paper by using the conceptual map shown in Fig. 9.

As the figure above shows, the starting point is the system of equations 3DA_1 (Eqs. (6) and (7)). The path on the left side is the usual way to solve the nonlinear second-order thermoviscous hydrodynamic model. For simplicity, we will focus on the one-dimensional problem 1DA_2 where the 1D Westervelt equation appears. To solve this system of equations for the unknowns u_z and p, in principle, one proceeds as follows: First of all, the 1D Westervelt equation (or its simplified version, the Burgers equation) must be solved to find the unknown $p(z,t)$. Then, to find the velocity $u_z(z,t)$ one must solve the first differential equation in 1DA_2 with the values of p found. This is a tedious process.

As an alternative way to the above, one can reduce the system 3DA_1 to the one dimensional form and apply finite difference to solve it numerically. But in this case, it is not possible to apply the Yee's mesh, at least, easily. As it is known, in the Yee's mesh the velocity $u_z(z,t)$ is defined on integer nodes of the space–time whereas the pressure $p(z,t)$ is defined on semi-integer nodes. The Yee's mesh is optimized in order to obtain higher computational performance. It has been proved that it is a very robust technique and remains at the core of many current FDTD softwares. So, it is recommended the use if the Yee's mesh.

In order to use Yee's mesh, we propose the following novel procedure (red path in the conceptual map Fig. 9):

(i) We use the substitution corollary in the proposed way (Eq. (10)) to obtain the system of equations 3DB_1. Using the substitution corollary for this purpose is novel in the literature.

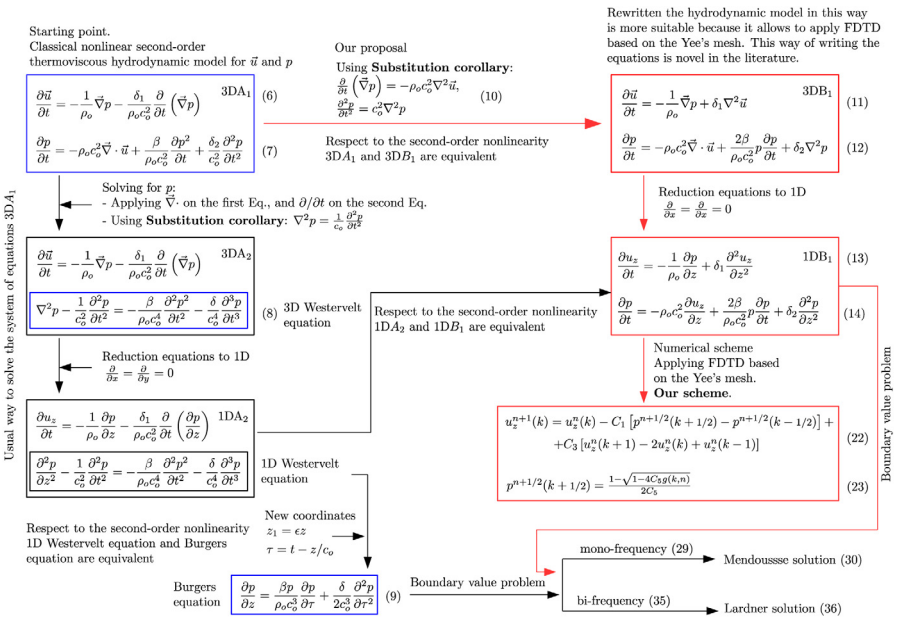

Fig. 9. Mathematical formulation developed in the paper.

(ii) The system of equations $3DB_1$ is original in the literature and it allows us to apply the Yee's mesh easily. So, one of the advantages of this formulation is to be able to apply the Yee's mesh without many difficulties.

(iii) As an example, we have discretized the system of equations $1DB_1$ (Eqs. (13) and (14)). The result is a robust and a compact scheme (Eqs. (22) and (23)) which allows us to get the unknowns u_z and p simultaneously without any extra effort. This is another advantage in relation to solve the Burgers equation first for p and then obtaining u_z.

(iv) Our scheme is a simple alternative to solve the one dimensional Westervelt equation or its simplified version, the Burger equation.

References

[1] Yee Kane. Numerical solution of initial boundary value problems involving maxwell's equations in isotropic media. IEEE Trans Antennas and Propagation 1966;14(3):302–7.

[2] Botteldooren D. Acoustical finite-difference time-domain simulation in a quasi-Cartesian grid. J Acoust Soc Am 1994;95(5):2313–9.

[3] Botteldooren Dick. Numerical model for moderately nonlinear sound propagation in three-dimensional structures. J Acoust Soc Am 1996;100(3):1357–67.

[4] LoVetri Joe, Mardare Doru, Soulodre Gilbert. Modeling of the seat dip effect using the finite-difference time-domain method. J Acoust Soc Am 1996;20.

[5] Botteldooren D. Finite-difference time-domain simulation of low-frequency room acoustic problems. J Acoust Soc Am 1995;98(6):3302–8.

[6] Renterghem Timothy, Botteldooren Dick. Numerical simulation of the effect of trees on downwind noise barrier performance. Acta Acust United Acust 2003;89:764–78.

[7] Redondo J, Picó R, Roig B, Avis MR. Time domain simulation of sound diffusers using finite-difference schemes. Acta Acust United Acust 2007;93(4):611–22.

[8] Hallaj Ibrahim M, Cleveland Robin O. FDTD simulation of finite-amplitude pressure and temperature fields for biomedical ultrasound. J Acoust Soc Am 1999;105(5):L7–12.

[9] Ginter Siegfried, Liebler Marko, Steiger Eckard, Dreyer Thomas, Riedlinger Rainer E. Full-wave modeling of therapeutic ultrasound: Nonlinear ultrasound propagation in ideal fluids. J Acoust Soc Am 2002;111(5):2049–59.

[10] Saeki Masaya, Bustamante Leslie, Misaki Takashi, Chiba Ko, Mano Isao, Nagatani Yoshiki, et al. FDTD simulation study of ultrasonic wave propagation in human radius model generated from 3D HR-pQCT images. Phys Med 2020;10:100029.

[11] Jiménez Nóe, Camarena Francisco, Redondo Javier, Sánchez-Morcillo Víctor, Hou, Yi, et al. Time-domain simulation of ultrasound propagation in a tissue-like medium based on the resolution of the nonlinear acoustic constitutive relations. Acta Acust United Acust 2016;102(5):876–92.

[12] Garrett SL. Understanding acoustics: an experimentalist's view of sound and vibration. Graduate texts in physics, Springer International Publishing; 2020.

[13] Shevchenko Igor, Kaltenbacher Barbara. Absorbing boundary conditions for nonlinear acoustics: The westervelt equation. J Comput Phys 2015;302:200–21.

[14] Westervelt Peter J. Scattering of sound by sound. J Acoust Soc Am 1957;29(2):199–203.

[15] Bonkile Mayur P, Awasthi Ashish, Lakshmi C, Mukundan Vijitha, Aswin VS. A systematic literature review of Burgers equation with recent advances. Pramana 2018;90(69):21.

[16] Dhawan S, Kapoor S, Kumar S, Rawat S. Contemporary review of techniques for the solution of nonlinear Burgers equation. J Comput Sci 2012;3(5):405–19, Advanced Computing Solutions for Health Care and Medicine.

[17] Enflo Bengt O, Hedberg Claes M. Theory of nonlinear acoustics in fluids. Springer Dordrecht; 2002.

[18] Jiwari Ram. Local radial basis function-finite difference based algorithms for singularly perturbed Burgers' model. Math Comput Simulation 2022;198:106–26.
[19] Jiwari Ram, Kumar Sanjay, Mittal RC. Meshfree algorithms based on radial basis functions for numerical simulation and to capture shocks behavior of Burgers' type problems. Eng Comput 2019;36(4):1142–68.
[20] Jiwari Ram. A hybrid numerical scheme for the numerical solution of the Burgers' equation. Comput Phys Comm 2015;188:59–67.
[21] Mittal RC, Pandit Sapna. Sensitivity analysis of shock wave Burgers' equation via a novel algorithm based on scale-3 Haar wavelets. Int J Comput Math 2018;95(3):601–25.
[22] Pandit Sapna, Kumar Manoj, Mohapatra RN, Alshomrani Ali Saleh. Shock waves analysis of planar and non planar nonlinear Burgers' equation using scale-2 haar wavelets. Internat J Numer Methods Heat Fluid Flow 2017;27(8):1814–50.
[23] Mur Gerrit. Absorbing boundary conditions for the finite-difference approximation of the time-domain electromagnetic-field equations. IEEE Trans Electromagn Compat 1981;EMC-23(4):377–82.
[24] Mendousse JS. Nonlinear dissipative distortion of progressive sound waves at moderate amplitudes. J Acoust Soc Am 1953;25(1):51–4.
[25] https://www.wolfram.com/mathematica/.
[26] Taflove A, Hagness SC. Computational electrodynamics: the finite-difference time-domain method. Artech house antennas and propagation library, Artech House; 2005.
[27] Lardner RW. Acoustic saturation and the conversion efficiency of the parametric array. J Sound Vib 1982;82(4):473–87, URL https://www.sciencedirect.com/science/article/pii/0022460X82904023.
[28] Hedberg Claes M. Multifrequency plane, nonlinear, and dissipative waves at arbitrary distances. J Acoust Soc Am 1999;106(6):3150–5.